Destructive testing and failure analysis of a full-scale composite tidal turbine blade

Fergus Cuthill, Sergio Lopez Dubon, Christopher Vogel, Miguel Valdivia Camacho, Conchúr Ó Brádaigh and Eddie McCarthy

***Abstract*—Tidal stream turbines play a pivotal role in harnessing marine energy, yet their reliability remains a critical challenge, impeding the cost-effectiveness of tidal energy. Deviations in blade performance can significantly impact turbine efficiency, potentially leading to unbalanced loads and consequential damage to the turbine and adjacent blades. Experience of blade failure, attributed to factors including material fatigue, manufacturing defects, environmental conditions, and operational stresses, underscores the urgency for comprehensive investigation and development of mitigation strategies. This study addresses these challenges by subjecting a composite tidal blade to a series of incremental static and fatigue tests, culminating in controlled failure experiments conducted at the FastBlade structural fatigue testing facility. The facility's advanced capabilities include a regenerative digital displacement hydraulic pump system yielding substantial energy savings; an advanced multi-camera digital image correlation system; and an acoustic emission crack detection system. Using these we systematically explore the factors contributing to blade failure. The failure modes examined in this study include: metal-composite bond failure; crack propagation in thick-section composites; and adhesive failure of the hydrodynamic outer skin. Our findings have significant implications for the structural engineering, composite material, and tidal energy development communities. Notably, our study offers valuable insights into the mechanisms underlying both blade failure under extreme loads and the accumulation of damage in large, thick composite structures. This research represents an important step towards enhancing the reliability and efficiency of tidal turbine blades, thus advancing the viability of tidal stream energy as a sustainable power source.**

***Index Terms*—Composites, Failure Analysis, Tidal energy, Tidal turbine Destructive Testing.**

Part of a special issue for ICOE 2024. Manuscript submitted 24 March 2025; Accepted 10 May 2025. Published 9 September 2025.

This work was supported in part by the SuperGen ORE Hub Flexible Fund Award FF2020-1063, the LoadTide Project

F. Cuthill is with the University of Edinburgh, FastBlade Test Centre, Edinburgh, UK (e-mail: Fergus.Cuthill@ed.ac.uk).

S. Lopez Dubon. is with the University of Edinburgh, Edinburgh, UK (e-mail: sergio.ldubon@ed.ac.uk).

C. Vogel is with the University of Oxford, Oxford, UK (email: christopher.vogel@eng.ox.ac.uk).

M. Valdivia Camacho is with the University of Edinburgh, Edinburgh, UK (e-mail: ma.valdivia@ed.ac.uk).

C. Ó Brádaigh was with the University of Edinburgh, Edinburgh, UK. He is now with The University of Sheffield, Sheffield, UK. (email: c.obradaigh@sheffield.ac.uk).

E. McCarthy is with the University of Edinburgh, Edinburgh, UK (e-mail: ed.mccarthy@ed.ac.uk).

Digital Object Identifier https://doi.org/10.36688/imej.8.279-285

I. Introduction

THE tidal industry has been slowly growing over the past decades with the first tidal stream turbine, a 300 kW device developed by Marine Current Turbines Ltd (MCT), being deployed in the ocean in May 2003 in north Devon, UK [1]. More recently, there has been much focus on scaling up and optimising the design of the turbines to reduce the levelised cost of energy in tide-generated currents. These new turbine designs include floating or seabed mounted units, with power ratings ranging from 2 kW up to 2 MW or higher. In 2023, the UK supported the tidal industry with Contracts for Difference (CfD) to install 50 MW of generating capacity, expecting new turbines online from 2027 [2]. The rise in both interest and funding for tidal turbine projects is pushing the need for development of the turbines themselves. Much of the powertrain technology can be transferred from wind power as they use similar generator technology [3]. The key parts that need to be developed to withstand the harsh marine environment are the turbine blades, foundations and mounting structures.

The FastBlade facility aims to address the development of the tidal turbine blades, offering static and fatigue testing to enable developers to refine their models, validate their designs and certify their blades. This serves to remove much of the uncertainty on how the blades respond to the extreme loads and fatigue cycling they will experience when deployed in the ocean.

Multiple tidal blades have been tested at facilities around the world such as the National Renewable Energy Laboratory (NREL) [4], the University of Gallway (UoG) [5], the University of Edinburgh (FastBlade) [6], the French Institute for Ocean Science (IFREMER) and the Technical University of Denmark (BLAEST) [7]. However, there are currently no published results detailing the structural failure of a full-scale composite tidal turbine blade and how the design choices, which have been made for the blade, may affect failure modes. At FastBlade, testing of a 5.2 m tidal blade, from a 500 kW turbine developed by Tidal Generation Limited (TGL), was carried out. The details of the test design and the results of the static and fatigue loading are presented in previous publications [6], [8]Testing at FastBlade was able to push the blade significantly beyond its design loads and achieve blade failure. The initial failure analysis is presented here with further analysis of the extensive data collected to be presented in future publications.

Fig. 1. DeepGen III Tidal turbine after being removed from the Fall of Warness site, showing the tidal blades, one of which was tested at FastBlade [9].

A. Abbreviations and acronyms

CfD – Contacts for Difference
CFRP – Carbon Fibre Reinforced Polymer
DIC – Digital Image Correlation
EMEC – European Marine Energy Centre
GFRP – Glass Fibre Reinforced Polymer
NREL – National Renewable Energy Laboratory
TGL – Tidal Generation Limited
MCT – Marine Current Turbines Ltd

II. LIFE OF THE BLADE

A. Manufacture

The tidal turbine blade tested in this project was supplied by the European Marine Energy Centre (EMEC). The blade was originally manufactured in November 2008 by Aviation Enterprises Ltd. The general structure of the blade featured a carbon fibre spar box, running from the root to near the tip of the blade. This was connected to a steel root connection by both bonding and clamping between the steel root connection disc and a central plug bolted within. The hydrodynamic shape was achieved by bonding glass fibre skins onto the carbon fibre spar using Spabond structural adhesive. The skins were also bonded together at both the leading and trailing edges, and along a series of stiffening ribs that act to link the skin to the carbon spar.

B. Installation at EMEC and storage in Orkney

The blade was installed on the 500 kW DeepGen III tidal turbine, deployed at EMEC in Orkney by TGL in September 2010; the full turbine can be seen in Fig 1. The turbine was grid-connected at the Fall of Warness test site in Eday. By March 2012 the turbine had generated over 200 MWh of electricity for the grid [10].

Following the successful deployment at EMEC, the turbine was later upgraded to 1 MW in January 2013 [11], this resulted in the blades from the 500 kW version lying in storage in Orkney as seen in Fig 2. The blades were stored uncovered, outdoors, for 8 years before being delivered to FastBlade in 2021 for testing. In 2016 Alstrom was acquired by GE and decided to suspend tidal turbine development. This has made it difficult to find accurate design and manufacturing documentation for the blade to aid in test design.

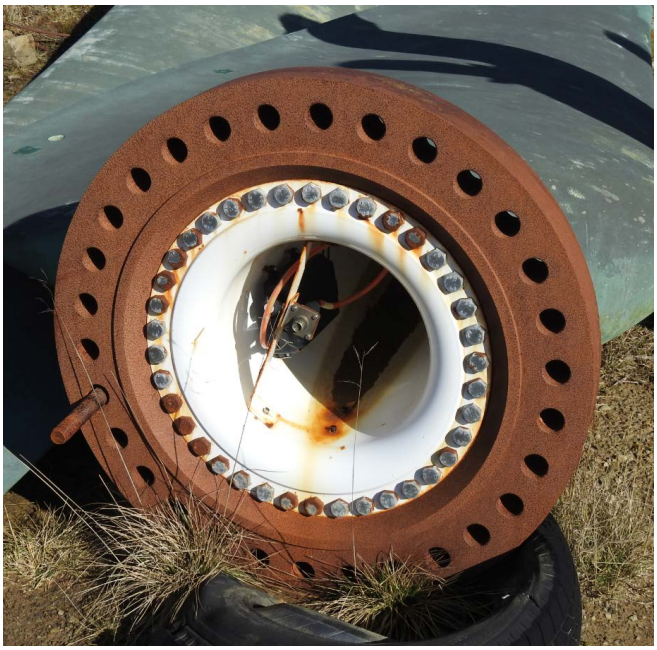

Fig. 2. 500 kW TGL Turbine blade stored outdoors in Orkney.

The aim of the testing at FastBlade was to perform a blade test programme meeting the ISO 62600-3 [12] standard to verify the blade could survive its design loads. In addition, hydrodynamic simulations of the turbine were carried out by Oxford University to provide updated loading distributions based on metocean data gathered at the Fall of Warness site at EMEC, as part of the ReDAPT Project, using two acoustic doppler current profilers [13], [14], [15], mounted to the new 1 MW turbine, after the 500 kW DeepGen III turbine was removed from the ocean. The simulations considered the ebb and flood tide vertical shear profiles observed across a range flow speeds during the tidal cycle. The updated hydrodynamic loadings provided by Oxford University were generated through simulations with their Actuator Line Model [16], and are used to generate a fatigue loading dataset, which would represent operating through 20 years of tidal cycles on the blade. The initial project focused on applying the design and simulated loads; however, after gathering all required data to meet the ISO 62600-3 standard, the test loads were increased until blade failure occurred.

III. STRUCTURAL TESTING

A. Test Facility Description

Testing was performed on the FastBlade main reaction frame shown in Fig 3, with multiple different loading setups, between April 2022 and April 2024. Full descriptions of the tests and loading setups used before failure can be found in [6], [8], [17], [18] The setup being discussed here, when blade failure occurred, featured three loading saddles, with angled actuators pushing in the XBB direction of the blade [6] as shown in Fig 3 and Fig 4.

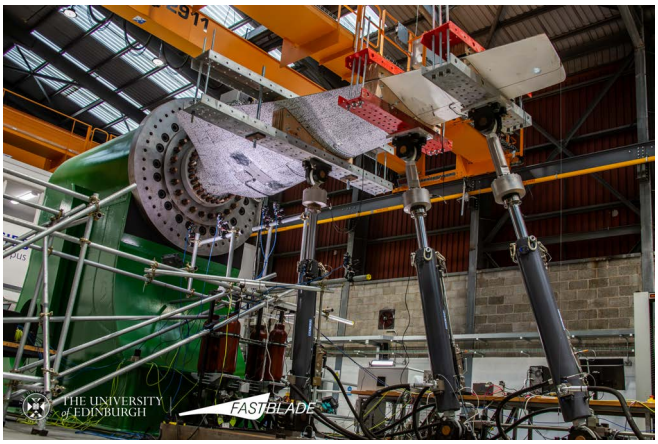

Fig. 3. TGL Blade undergoing testing at FastBlade.

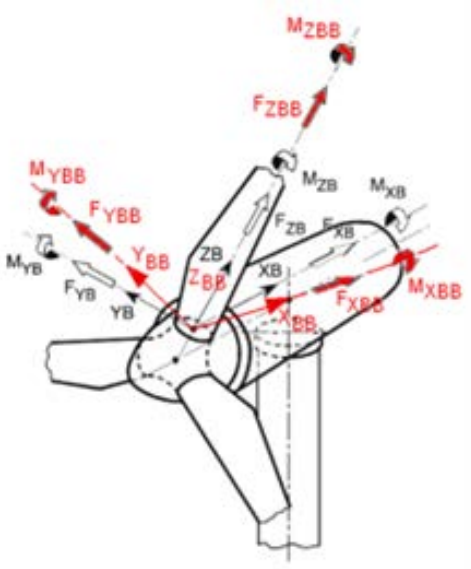

Fig. 4. Blade Axis System referenced during testing at FastBlade [6].

B. Test Definition

Although multiple different actuator setups were used at different times throughout the testing, the root bending moment for the blade was always the target for the load cases.

Static loading was based on the extreme case specified in the design documents from the simulations carried out by TGL in 2008. This load case was based on a 50 year tidal current peak velocity of 4.1 m/s and a 50 year wave peak height of 11.2 m. The target bending moment for static loading was 974.7 kN.m, achieved with 3 actuators acting in the XBB direction, targeting 94.4 kN at distances of 2.27 m, 3.57 m, and 4.47 m from the blade root. Fatigue loading was based on the simulations carried out by Oxford University at the mean flow speed of the test site (2.8 m/s). The target bending moment for this load case was 670 kN.m. With the same actuator positions as above the target peak actuator load was 65 kN. Fatigue loading was then carried out at the static extreme load case of 974.7 kN.m. When no failure was detected at this level, static loading was increased until the first failure occurred at the blade root.

Fig. 5. Installation of Strain gauges around hole and notches in the blade.

The aim of the above configuration was to direct failure to occur in the main composite body of the blade, rather than continuing to push the debonding of the skin at the root of the blade. In order to achieve this, a structural defect was introduced into the blade to act as a stress concentration to force failure to occur within the composite. A 25 mm diameter hole was drilled into the composite in line with the centre of the blade root, in the direction of the XBB axis at 100 mm past the end of the steel insert (approximately 1.2 m from the root of the blade). This location was chosen as it was close enough to the root that large bending moments being transferred through the area should result in significant stress concentration with the influence of the steel root connection minimised. A series of linear strain gauges were placed around the hole to monitor strain levels at the stress concentration. The gauges were orientated in line with the longitudinal (ZBB) axis of the blade of the blade and at 90° spacings around the hole. Four static tests were carried out, reaching a peak load of 94.43 kN on each of the three actuators, resulting in a root bending moment of 974.4 kN.m.

When the strain level around the hole was noted to be 0.156 % and no failure around the hole was observed, notches were cut into the blade using the hole as the centre point with 100 mm notches extending towards the leading and trailing edges of the blade at 90° to the longitudinal axis of the blade. Strain gauge rosettes were applied approximately 50 mm from the tip of the notch; the gauge setup can be seen in Fig 5. This was to enable DIC speckle to be applied all around the tip of the notch, so that a full strain field could be determined, rather than just localised strain measurements from the gauges.

Static and fatigue testing were once again carried out, finishing with a cyclic fatigue test featuring peak loads of 774 kN.m, and a peak strain was measured 50 mm from the notch at 0.95 % strain without failure, while avoiding overloading the root. Thus, to further promote failure, the notches were extended to +/- 200 mm from the hole, cutting entirely through one side of the carbon fibre spar. New strain gauges were applied

Fig. 6. Image of failed blade root showing crack from delamination extending around the circumference of root connection.

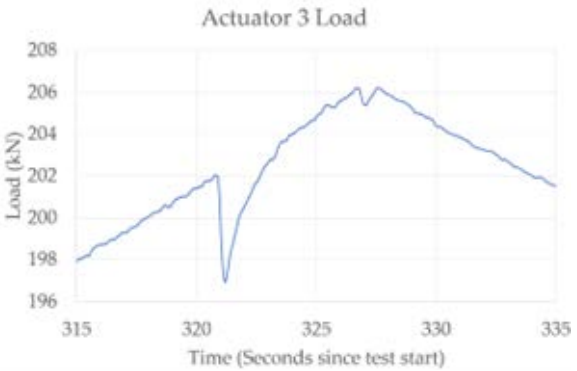

Fig. 7. Graph showing 5 kN load drop during root failure, followed by further cracking and subsequent test halt.

at 10 mm from the tip to obtain a real-time readout of accurate strain near the tip. These notches resulted in a new load path to the root of the blade where the majority of the bending moment was transferred via the skin near the leading and trailing edges of the blade. Blade failure occurred during fatigue cycling with a peak root bending moment of 774.16 kN.m after 2500 cycles with a load ratio of R = 0.26. The high strain levels where the strain gauges were installed caused them to fail, so reliable strain gauge readings at this location are not available.

IV. Blade Failure

A. Root Failure

described in the timeline of blade testing above, the first detectable failure occurred at the root of the blade. The failure initially appeared as a debond between the glass fibre skin of the blade and the steel root connection, as shown in Fig 7. The failure occurred during a static test, targeting an actuator load of 220 kN at a loading rate of 1.467 kN/s; during the ramping, failure in the root occurred at 200.3 kN, with an average load drop of 5 kN on each of the 3 actuators. Nevertheless, the test was continued, as the load appeared to recover and stabilise after the initial failure; however, after a further failure at 206.2 kN, it was decided to stop the test for inspections. A graph showing the initial load drop for a single actuator can be seen in Fig 6. After the inspections identified the delamination root failure, the test was repeated, and the load of 220 kN was achieved and held for 150 seconds with no further failures detected. After this test, the decision was made to attempt to initiate a crack failure in the blade, as the first failure mode had been identified, and it was believed that pushing further would have resulted in further failures at the root with little extra information gathered about other areas of the blade.

B. Stress Concentration Hole

After the hole was drilled in the blade, a series of static ramps were performed, investigating the strain level around the hole, without approaching the load level, which might have caused further root failure. After further investigation, no failure was detected, and the strain level was too low at the edges of the hole to cause failure in a reasonable timeframe.

C. Stress Concentration Notches

After the series of static tests and small fatigue tests, no failure or crack propagation from the edge of the 100 mm notches was detectable with imaging or DIC results. Although the strain level measured at one of the notches in the 0° direction (longitudinally down the blade) was measured to be 0.95 %, the other notch showed a strain of 0.5 %; thus, the decision was made to extend the notches to further accelerate failure. A graph showing the strain rise throughout a static test reaching a peak strain of 0.95 % can be seen in Fig 8.

D. Stress Concentration Notch Extensions

With the large 200 mm notches in the blade skin and spar, at the time of testing, it was not completely clear whether the spar had been fully cut due to the difficulty of inspecting the 80+ mm thick composite, however, the strain gauges placed near the notch tips indicated high levels of strain, and during a fatigue test, the cyclic loading resulted in strain gauge failure due to fatigue. Gauges had to be reinstalled further from the notch, and the DIC imaging was used for strain analysis. With the large notches, composite cracking occurred in the surface of the composite, which was detected in the DIC images.

E. Ultimate failure at seam

The final failure of the blade occurred during fatigue testing, where the aim was to further progress the cracks that had been detected at the notch tips. The bonded seam between the top and bottom skins of the blade, along the leading edge, suffered catastrophic debonding, with approximately 1 m of seam bursting open in less than 0.1 seconds. This seam then continued to open until the clamping force of the loading saddle restricted its further propagation along the leading edge. The seam burst on the cycle before the test was stopped, meaning the reduction in stiffness of the blade

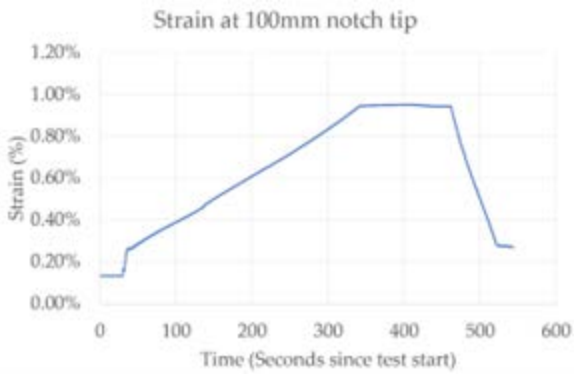

Fig. 8. Strain at notch closest to blade trailing edge in the 0° (longitudinal) direction reaching a peak of 0.95 % strain.

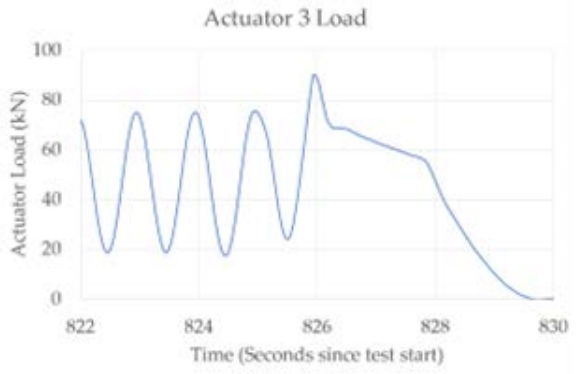

Fig. 9. Graph showing load during blade seam failure, failure happened before peak load is reached causing control system to ramp up to compensate for failure, resulting in the measured peak load of 90.26 kN.

resulted in the control system increasing the oil flow required to deliver the additional displacement of the actuators. This resulted in an overshoot of the target load as seen in Fig. 9, with the test system reaching a limit state and shutting down. The seam failure near the leading edge of the blade is shown in Fig 10.

F. Residual strength test

After the blade seam failure had been analysed and imaged, further testing was carried out to investigate the residual strength of the blade. A static test with a ramp rate of 6.5 kN/min aimed to reach 65 kN per actuator (matching the designed fatigue strength of the blade), however, at 58 kN further failure was detected as the split in the skin seam continued extending, past the section of the blade which was clamped by the saddle. The tip deflection at this load was 343.3 mm, a 255 % increase in deflection compared to a tip deflection of 96.8 mm before any detectable damage had occurred at the same load.

G. Reduction in Natural frequency

After all the tests and analyses of the blade had been completed, the loading saddles and actuators could be taken down. The removal of all the connections made it possible to carry out a natural frequency test to determine to what extent the damage had compromised the structure of the blade and caused a reduction in stiffness. The natural frequency of the blade when it was received at FastBlade was 18.03 Hz and after all the testing and damage, the frequency was reduced to 14.62 Hz.

Fig. 10. Image showing blade seam failure at the overlap where the top and bottom skins of the material were bonded.

V. FAILURE ANALYSIS AND DISCUSSION

A. Delamination of root composite/steel plug

The delamination that occurred between the steel root plug and the composite skin was the first failure mode that was detectable in the turbine blade, without artificial influence from stress holes/notching. However, this failure may have been influenced by the service and storage conditions of the blade; as can be seen in Fig 2, the root section of the blade was coated with rust after years of storage. This rust may have extended into the bonded area between the skin and the steel, resulting in reduced bond strength and the resulting failure. Rusting can be a major concern while a blade is deployed in the ocean, but regular inspection, with rust prevention techniques and coatings, may have prevented extensive rusting of this blade. After the root debond failure occurred, the blade was still capable of withstanding the design fatigue and ultimate load cases, so it is not expected that this failure would have been catastrophic for a blade in service, and it may have been repairable.

B. Crack propagation at notch tips

The crack propagation within the blade skin at the tip of the notches is a result of the extremely high strain levels detected, due to the stress concentration introduced during the testing. The failure in the composite surface is visible in Fig 11. It is possible that this sort of failure could propagate from areas on the blade, which already have defects such as manufacturing faults or impact damage during service. Failure, in this blade by this mechanism, however, appears to be unlikely due to the extreme nature of the notching that was required to initiate this failure. An entirely different load path through the skins was required, rather than through the carbon fibre spar, to achieve strain levels high enough to cause this failure.

Fig. 11. Visible cracking in composite surface running at 45° from the tip of the notch. Ruler and notch at image right orientated in chordwise direction.

Fig. 12. Thick adhesive layers (green) averaging 10 mm thickness, showing debonding from the GFRP blade skin.

C. O. Split at skin bond line

The most significant failure, relevant to the blade in service, is the debonding of the adhesive at the bond line along the leading edge of the blade. In the testing at FastBlade, however, this failure likely occurred due to the machined notch weakening the blade and altering the load path to the root as no significant strain was noted along the leading edge before the notches were cut in the blade. Manufacturing issues or debonding of the adhesive between the spar and skins could easily result in this load path through the skin being a likely failure mode for the blade. If this blade failed in this way during service, it is unlikely that any repair would be possible due to the difficulty in re-establishing a good bond between the skins and the inability to inspect or repair any bonding issues anywhere else in the blade.

D. Contributing factors to blade failures

After the testing and visual inspection of the blade had been completed, various panels were cut out of the blade skin and spar to allow inspection and analysis of the internal structure of the blade. Based on the available data, several key factors may have contributed to the performance of the blade during testing.

1) Thick adhesive layers: Thick adhesive layers, bonding the skin to ribs and spar, measured at more than 20 mm in some places and averaging over 10 mm. These layers were thicker than expected according to all the manufacturing documentation available. This may have resulted in different stiffness and performance compared to the expected GFRP and CFRP components. An image of the Spabond adhesive can be seen in Fig 12.

2) Inadequate bonding between the Spabond adhesive and the skin: As the panels of the blade were cut out for inspection, there appeared to be a very weak bond to the skin, with only a slight lever action with a pry bar causing the entire skin panel to release from the adhesive, inspecting the underside of the panel, it was clear that only about 10 % of the skin was adequately bonded to the internal structure. This can be seen in Fig 13 where large areas of the GFRP skin panels do not show any indication of adhesive bonding.

Fig. 13. Cut away blade skin showing inadequate bonding between the blade skin and core structure.

3) Incorrect bond areas: 3) Along the skin bond at the leading edge, the manufacturing drawings indicated a full structural bond throughout the entire overlapped area, however, when inspecting the failed edge, it was found that only approximately 50 % of the overlap was bonded, the rest appeared to be a non-structural filler. This was likely required due to issues encountered when attempting to assemble the blade but will have reduced the strength along the leading-edge bond significantly. A cutaway section of the blade from the leading edge bond to the carbon spar can be seen in Fig 14.

4) Adhesive voids: Where the adhesive is used in the blade, there are large voids where the adhesive has not fully spread to cover the area under the skin. Fig 15 shows this, where it appears that the adhesive was applied in lines, expecting the compression of the skin to spread the adhesive correctly. This likely resulted in reduced bond strength and stress concentration along the numerous additional bond edge voids.

5) Layup variations: The laminate layup measured in the blade does not match that of the available manufacturing drawings. Variations up to 500 % increase in laminate thickness in places were noted. This may have contributed to the blade outperforming its ultimate

Fig. 14. Image showing a section of blade with the outer skin removed. From bottom to top: leading edge of blade, pink coloured filler at overlap seam, green Spabond adhesive, black carbon spar.

Fig. 15. Section through blade skin showing voids in between adhesive bond lines. Adhesive thickness at this location is approximately 15 mm.

load cases by such a large amount and may have offset some of the other manufacturing issues mentioned above.

VI. Conclusions

This work has demonstrated the first failure mode a tidal turbine blade with this design may encounter under similar load conditions to its design load cases. Which is a debond between the metallic and composite components. This was followed by several induced failures as part of the study at FastBlade. In addition, the following points can be noted regarding the design and manufacture of the blade used during this study. The blade appears to be overbuilt with a conservative design, withstanding more than double its most extreme static design load case and more than 3 times the rated load case, and still resisting a large proportion of its fatigue load case even after multiple failures and weaknesses in the blade were introduced. The deviations from the manufacturing documentation are a huge challenge for modelling and understanding the blade behaviour. A clear understanding of the test specimen is required to properly design structural tests and understand the outcomes of the testing, as it was not possible to predict failure modes based on the preliminary modelling of the turbine blade. Although the study presented here is specific to this turbine blade, the issues relating to root connection failure, delamination, achieving desired adhesive bond strength and the failure of adhesive bonds throughout a blade will be relevant to almost all tidal turbine blade designs.

VII. References

References

[1] G. Marsh, "Tidal turbines harness the power of the sea," *Reinforced Plastics*, vol. 48, pp. 44–47, 2004. [Online]. Available: https://www.sciencedirect.com/science/article/pii/S0034361704003443

[2] A. Garanovic, "UK supports 11 tidal energy projects with record capacity of over 50MW in latest CfD auction round," 2023.

[3] D. Coles, A. Angeloudis, Z. Goss, and J. Miles, "Tidal stream vs. wind energy: The value of cyclic power when combined with short-term storage in hybrid systems," *Energies*, vol. 14, 2021. [Online]. Available: https://www.mdpi.com/1996-1073/14/4/1106

[4] R. E. Murray, R. Beach, P. Murdy, S. Dana, and S. Hughes, "Structural characterization of deployed thermoplastic and thermoset composite tidal turbine blades," National Renewable Energy Laboratory, Tech. Rep., 2024.

[5] Y. Jiang, W. Finnegan, F. Wallace, M. Flanagan, T. Flanagan, and J. Goggins, "Structural analysis of a fibre-reinforced composite blade for a 1 MW tidal turbine rotor under degradation of seawater," *Journal of Ocean Engineering and Marine Energy*, vol. 9, pp. 477–494, 2023. [Online]. Available: https://doi.org/10.1007/s40722-023-00279-w

[6] S. Dubon, F. Cuthill, C. Vogel, C. Ó Brádaigh, and E. McCarthy, "A full-scale composite tidal blade fatigue test using single and multiple actuators," *Composites Part A: Applied Science and Manufacturing*, vol. 181, p. 108140, 6 2024.

[7] T. R. M. Thanthirige, J. Goggins, M. Flanagan, and W. Finnegan, "A state-of-the-art review of structural testing of tidal turbine blades," *Energies*, vol. 16, 2023. [Online]. Available: https://www.mdpi.com/1996-1073/16/10/4061

[8] S. Dubon, C. Vogel, D. Cava, F. Cuthill, E. McCarthy, and C. Ó Brádaigh, "Multi-actuator full-scale fatigue test of a tidal blade," in *EWTEC, vol. 15*, 2023.

[9] D. R. Noble, "The 500 kW TGL DeepGen III tidal stream turbine at Hatston Pier, Orkney," 2014.

[10] E. M. E. C. (EMEC), "Emec clients/alstom (formerly tgl)." [Online]. Available: https://www.emec.org.uk/about-us/our-tidal-clients/alstom/

[11] E. T. Institute, "Energy Technologies Institute (ReDAPT project)." [Online]. Available: https://tidalenergydata.org/projects/detail/ReDAPT

[12] I. E. Commission, "IEC 62600-3 marine energy - wave, tidal and other water current converters - part 3: Measurement of mechanical loads," International Electrotechnical Commission, Tech. Rep., 5 2020.

[13] B. Sellar and D. Sutherland, "Tidal energy site characterisation at the Fall of Warness, EMEC, UK," University of Edinburgh, Tech. Rep., 2016.

[14] B. Sellar, "Metocean data set from the ReDAPT tidal project: Batch 1, part 2," University of Edinburgh. School of Engineering, Tech. Rep., 2017.

[15] B. G. Sellar, G. Wakelam, D. R. J. Sutherland, D. M. Ingram, and V. Venugopal, "Characterisation of tidal flows at the european marine energy centre in the absence of ocean waves," *Energies*, vol. 11, 2018. [Online]. Available: https://www.mdpi.com/1996-1073/11/1/176

[16] A. Wimshurst and R. Willden, "Validation of an actuator line method for tidal turbine rotors," in *Validation of an Actuator Line Method for Tidal Turbine Rotors*, 3 2016.

[17] S. Dubon, C. Vogel, D. Cava, F. Cuthill, E. McCarthy, and C. Ó Brádaigh, "A full-scale tidal blade fatigue test using the FastBlade facility," *Renewable Energy*, vol. 228, p. 120653, 7 2024.

[18] S. Dubon, C. Vogel, D. Cava, F. Cuthill, E. McCarthy, and C.M. Ó Brádaigh, "FastBlade: A technological facility for fullscale tidal fatigue testing," in *SAMPE 2023 — SEATTLE, WA*, 6 2023.